Effects of Ring Tilting on Rates of Intramolecular Electron Transfer in Mixed-Valence 1′,2′,1‴,2‴-Tetraethyl-, 1′,3′,1‴,3‴-Tetraethyl-, and 1′,2′,4′,1‴,2‴,4‴-Hexaethylbiferrocenium Triiodides

Teng-Yuan Dong,*[1] Chun-Hsun Huang,[1,2] Chung-Kay Chang,[1,3] Yuh-Sheng Wen,[1] Shyi-Long Lee,*[1] Jinq-An Chen,[1] Wen-Yann Yeh,[2] and Andrew Yeh[3]

Contribution from the Institute of Chemistry, Academia Sinica, Nankang, Taipei, Taiwan, ROC, Department of Chemistry, National Sun Yat-sen University, Kaohsuing, Taiwan, ROC, and Department of Chemistry, Chung-Yuan Christian University, Chung-Li, Taiwan, ROC

Received November 9, 1992

Abstract: Relatively minor perturbations caused by Cp ring substituents in a series of mixed-valence biferrocenium cations have pronounced effects on the electronic structure and rate of intramolecular electron transfer. The X-ray structure of 1′,2′,1‴,2‴-tetraethylbiferrocene has been determined at 298 K: $C2/c$, a = 18.760(3) Å, b = 9.568(3) Å, c = 16.441(3) Å, β = 130.494(13)°, Z = 4, D_{calcd} = 1.42 g cm^{-1}, R_f = 0.038, and R_{wf} = 0.041. The isomeric compound 1′,3′,1‴,3‴-tetraethylbiferrocene crystallizes in the triclinic space group $P\bar{1}$ with one molecule in a unit cell with dimensions a = 5.8649(6) Å, b = 8.8462(6) Å, c = 12.4822(11) Å, α = 109.814(6)°, β = 103.063(8)°, and γ = 83.476(6)°; R_f = 0.046, and R_{wf} = 0.055. The mixed-valence compound 1′,3′,1‴,3‴-tetraethylbiferrocenium triiodide crystallizes in the triclinic space group $P\bar{1}$ with one molecule in a unit cell with dimensions a = 8.4567(20) Å, b = 9.0268(15) Å, c = 10.9182(12) Å, α = 105.777(12)°, β = 101.606(13)°, and γ = 106.301(15)°; R_f = 0.042, and R_{wf} = 0.042. A three-dimensional hydrogen bonding network is clearly found between the Cp ring hydrogen atoms and iodine counterion atoms. The two crystallographically equivalent metallocene moieties of the cation have dimensions intermediate between those of Fe^{II} and Fe^{III} metallocenes. The variable-temperature ^{57}Fe Mössbauer data indicate that there is a pronounced dependency on sample history for 1′,1‴-diethyl-, 1′,2′,1‴,2‴-tetraethyl-, and 1′,3′,1‴,3‴-tetraethylbiferrocenium triiodides. Crystalline samples of 1′,2′,1‴,2‴-tetraethyl- and 1′,3′,1‴,3‴-tetraethylbiferrocenium triiodide are delocalized on the Mössbauer time scale in the solid state above 195 and 125 K, respectively. We suggest that the difference in the rates of electron transfer in the series of mixed-valence biferrocenium salts is a result of difference in the degree of tilting of the Cp rings from the parallel geometry. Deviations of the Cp rings from the parallel position were found to correlate quite well with the critical temperature for electronic delocalization–localization in mixed-valence biferrocenium salts. Based on extended Hückel MO calculations, a theoretical explanation of the influence of bending back the Cp rings on the electron-transfer rates is also presented.

Introduction

The study of intramolecular electron transfer in mixed-valence complexes has enabled systematic and creative investigations into the factors that affect rates of electron transfer in solution redox processes, solid-state materials, and biological electron-transfer chains.[4-7] The two most thoroughly studied mixed-valence complexes are the ruthenium amine complexes[7] and the binuclear biferrocenium salts.[8]

In the case of mixed-valence biferrocenium triiodide salts **1–13** (Scheme I), considerable progress has been made in understanding the effects of the solid-state environment on the rate of electron transfer.[9-15] When there is an onset of dynamics associated with the counterions, or ligands, this will probably influence the rate of intramolecular electron transfer. Very recently, it has been found[16] that changing the substituent in the benzyl unit in compounds **6–10** leads to dramatic changes in the electron-transfer

Scheme I

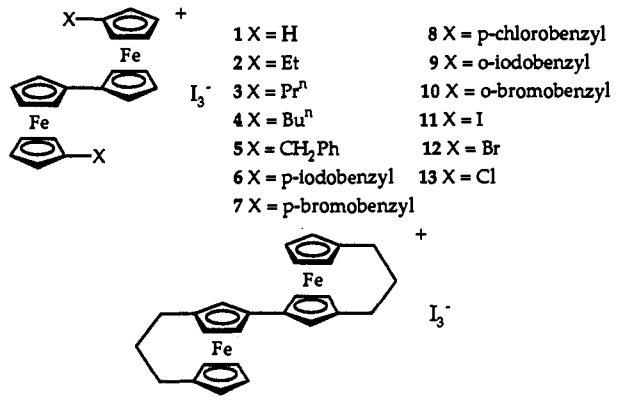

14

(1) Institute of Chemistry, Academia Sinica.
(2) Department of Chemistry, National Sun Yat-sen University.
(3) Department of Chemistry, Chung-Yuan Christian University.
(4) Day, P. *Int. Rev. Phys. Chem.* **1981**, *1*, 149.
(5) Brown, D. *Mixed-Valence Compounds, Theory and Applications in Chemistry, Physics, Geology and Biology*; Reidel: Boston, MA, 1980.
(6) Creutz, C. *Prog. Inorg. Chem.* **1983**, *30*, 1.
(7) Richardson, D. E.; Taube, H. *Coord. Chem. Rev.* **1984**, *60*, 107.
(8) Hendrickson, D. N.; Oh, S. M.; Dong, T.-Y.; Kambara, T.; Cohn, M. J.; Moore, M. F. *Comments Inorg. Chem.* **1985**, *4*, 329.
(9) Dong, T.-Y.; Hendrickson, D. N.; Iwai, K.; Cohn, M. J.; Geib, S. J.; Rheingold, A. L.; Sano, H.; Motoyama, I.; Nakashima, S. *J. Am. Chem. Soc.* **1985**, *107*, 7996.
(10) Dong, T.-Y.; Hendrickson, D. N.; Pierpont, C. G.; Moore, M. F. *J. Am. Chem. Soc.* **1986**, *108*, 963.
(11) Iijima, S.; Saida, R.; Motoyama, I.; Sano, H. *Bull. Chem. Soc. Jpn.* **1981**, *54*, 1375.
(12) Nakashima, S.; Katada, M.; Motoyama, I.; Sano, H. *Bull. Chem. Soc. Jpn.* **1987**, *60*, 2253.
(13) Kai, M.; Katada, M.; Sano, H. *Chem. Lett.* **1988**, 1523.
(14) Dong, T.-Y.; Schei, C. C.; Hsu, T. L.; Lee, S. L.; Li, S. J. *Inorg. Chem.* **1991**, *30*, 2457.
(15) Dong, T.-Y.; Chou, C. Y. *J. Chem. Soc., Chem. Commun.* **1990**, 1332.
(16) Dong, T.-Y.; Schei, C. C.; Hwang, M. Y.; Lee, T. Y.; Yeh, S. K.; Wen, Y. S. *Organometallics* **1992**, *11*, 573.

0002-7863/93/1515-6357$04.00/0

Scheme II. Reagents and conditions: i, $AcCl/AlCl_3$; ii, $LiAlH_4/AlCl_3$; iii, activated Cu; iv, I_2

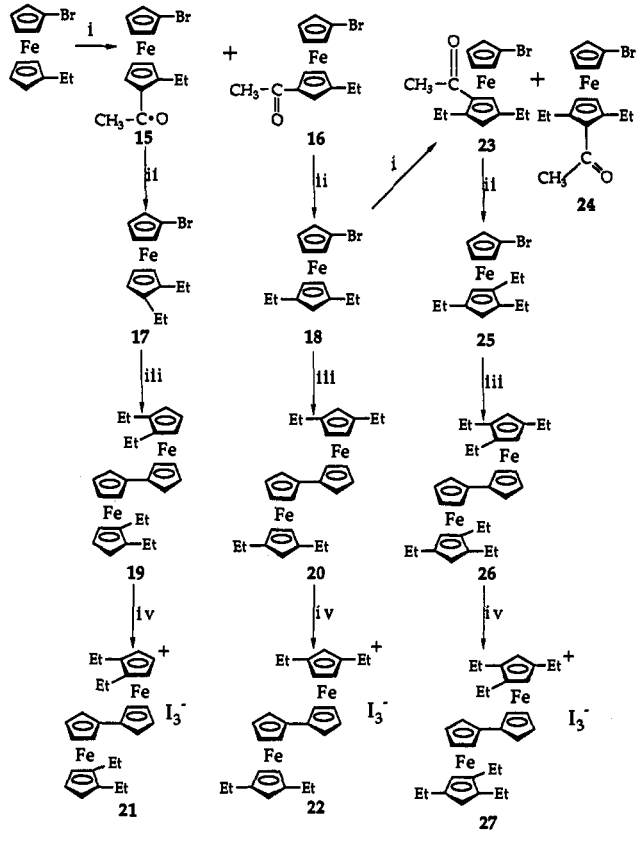

rate in the solid state. The interactions between the cation and anion undoubtedly alter the potential energy surface of the mixed-valence molecule and therefore rate of intramolecular electron transfer. Recently, Hendrickson and co-workers have addressed counterion effects on intramolecular electron-transfer rates of biferrocenium salts.[17-20] The size, shape, and charge distribution of anions can ultimately affect the solid-state arrangement adopted by a particular system. Perhaps the best characterized examples of the environmental control of intramolecular electron-transfer rates are found in the case of the mixed-valence trinuclear iron acetate complexes, where the onset of solvate molecule dynamics in the solid state triggers a dramatic increase in the electron-transfer rate.[21,22]

A recent interesting finding is that there is a significant influence on the electron-transfer rate in the mixed-valence biferrocenium salt **14** when the cyclopentadienyl (Cp) rings in the ferrocenyl moieties are linked by an interannular trimethylene bridge.[15,23] In our previous papers,[23,24] we proposed that such a structural modification would lead to increased metal–ligand interactions as the rings tilt.

To study the influence of tilting the Cp rings in compounds **1–13**, we have prepared a series of polyethylbiferrocenium triiodide salts (Scheme II). Furthermore, we have performed extended Hückel MO calculations on biferrocenium triiodide, **1**, for different dihedral angles between the two Cp rings to elucidate the geometric effect on the rates of intramolecular electron transfer in mixed-valence biferrocenium cations.

Experimental Section

General Information. All manipulations involving air-sensitive materials were carried out by using standard Schlenk techniques under an atmosphere of N_2. Chromatography was performed on neutral alumina (activity II), eluting with hexane/CH_2Cl_2. Dichloromethane was dried over P_2O_5. The sample of 1-ethyl-1′-bromoferrocene was prepared according to the literature procedure.[25]

Acetylation of 1-Ethyl-1′-bromoferrocene. The acetylating reagent was made-up according to the Friedel–Crafts synthesis by mixing 0.548 mL (8.09 mmol) of acetyl chloride and excess $AlCl_3$ in dry CH_2Cl_2 (100 mL) at 0 °C under N_2. The excess of $AlCl_3$ was filtered off with glass wool.

The acetylating reagent was added by means of a dropping funnel over a period of about 1 h to a solution of 1-ethyl-1′-bromoferrocene (2.37 g, 8.09 mmol) in dry CH_2Cl_2 (100 mL) at 0 °C. The reaction mixture was stirred for 2 h and then poured into an ice–water mixture. The resulting mixture was separated after the reduction of ferrocenium cation with aqueous $Na_2S_2O_3$. The organic layer was washed with saturated aqueous $NaHCO_3$ and with water, and then it was dried over $MgSO_4$. The solvent was removed under reduced pressure. The red oily residue was chromatographed. The first band eluted with *n*-hexane/CH_2Cl_2 (7:3) was the starting material. The second band was a mixture of **15** and **16**. This mixture could be separated by rechromatographing on silica gel (70–230 mesh) using *n*-hexane/ethyl acetate (15:1) as the eluent. The first band was **15** (18%) and the second band was **16** (22%). The properties of **15** are as follows. ^1H NMR ($CDCl_3$, ppm): 1.11 (t, 3H, $-CH_3$), 2.35 (s, 3H, $-COCH_3$), 2.62 (m, 2H, $-CH_2-$), 3.96 (t, 1H, Cp), 4.00 (t, 1H, Cp), 4.26 (t, 2H, Cp), 4.35 (t, 2H, Cp), 4.54 (t, 1H, Cp). Mass spectrum: M^+ at m/z 335. The properties of **16** are as follows. ^1H NMR ($CDCl_3$, ppm): 1.19 (t, 3H, $-CH_3$), 2.35 (s, 3H, $-COCH_3$), 2.35 (q, 2H, $-CH_2-$), 4.01 (t, 1H, Cp), 4.06 (t, 1H, Cp), 4.27 (t, 2H, Cp), 4.39 (q, 1H, Cp), 4.69 (m, 2H, Cp). Mass spectrum: M^+ at m/z 335.

Reduction of 15 and 16. The reduction reaction was carried out by carefully adding, with stirring, small portions of $AlCl_3$ to a mixture of the ferrocene compound and $LiAlH_4$ in dry ether. After 30 min, the solution became yellow, an excess of H_2O was added to it, and the ether layer was separated. The ether layer was washed with H_2O and dried over $MgSO_4$. After evaporation of the solvent, the crude product was chromatographed on Al_2O_3, eluting with hexane. The first band was the desired compound. The yields were approximately 85%. The physical properties of **17** are as follows. ^1H NMR ($CDCl_3$, ppm): 1.14 (td, 6H, $-CH_3$), 2.37 (m, 4H, $-CH_2-$), 3.96 (d, 2H, Cp), 4.03 (m, 3H, Cp), 4.06 (t, 1H, Cp), 4.18 (d, 2H, Cp). Mass spectrum: M^+ at m/z 320. The physical properties of **18** are as follows. ^1H NMR ($CDCl_3$, ppm): 1.21 (t, 6H, $-CH_3$), 2.36 (m, 4H, $-CH_2-$), 4.03 (m, 5H, Cp), 4.24 (dd, 2H, Cp). Mass spectrum: M^+ at m/z 320.

Ullmann Reaction of 17 and 18. A mixture of the corresponding bromoferrocene (1 g) and activated copper (5 g) was heated under N_2 at 110–120 °C for 24 h. After cooling to room temperature, the reaction mixture was repeatedly extracted with CH_2Cl_2 until the CH_2Cl_2 extracts appeared colorless. The extracts were evaporated and chromatographed. The first band eluted with hexane yielded the starting material. Continued elution with hexane afforded the desired compound. Compounds **19** and **20** were recrystallized from hexane. The yields were approximately 70%. ^1H NMR of **19** ($CDCl_3$, ppm): 1.01 (t, 12H, $-CH_3$), 2.08 (q, 8H, $-CH_2-$), 3.77 (d, 2H, Cp), 3.82 (d, 4H, Cp), 4.05 (t, 4H, Cp), 4.14 (d, 4H, Cp). Mp: 46.7–47.5 °C. Mass spectrum: M^+ at m/z 482. ^1H NMR of **20** ($CDCl_3$, ppm): 1.03 (t, 12H, $-CH_3$), 2.11 (q, 8H, $-CH_2-$), 3.73 (s, 6H, Cp), 4.05 (t, 4H, Cp), 4.14 (d, 4H, Cp). Mp: 75.3–76.4 °C. Mass spectrum: M^+ at m/z 482.

Acetylation of 18. The Friedel–Crafts reaction of **18** was carried out according to the same procedure as the acetylation of 1-ethyl-1′-bromoferrocene. The red oily residue was chromatographed on alumina. The first band eluted with hexane/CH_2Cl_2 (7:3) was the recovered starting material. The second band was a mixture of **23** and **24**. Similarly, this mixture could be separated into three bands upon rechromatographing on silica gel with hexane/ethyl acetate (15:1) as the eluent. The first and

(17) Webb, R. J.; Geib, S. J.; Staley, D. L.; Rheingold, A. L.; Hendrickson, D. N. *J. Am. Chem. Soc.* **1990**, *112*, 5031.
(18) Webb, R. J.; Rheingold, A. L.; Geib, S. J.; Staley, D. L.; Hendrickson, D. N. *Angew. Chem., Int. Ed. Engl.* **1989**, *28*, 1388.
(19) Dong, T.-Y.; Kambara, T.; Hendrickson, D. N. *J. Am. Chem. Soc.* **1986**, *108*, 5857.
(20) Dong, T.-Y.; Kambara, T.; Hendrickson, D. N. *J. Am. Chem. Soc.* **1986**, *108*, 4423.
(21) Jang, H. G.; Geib, S. J.; Kaneko, Y.; Nakano, M.; Sorai, M.; Rheingold, A. L.; Montez, B.; Hendrickson, D. N. *J. Am. Chem. Soc.* **1989**, *111*, 173.
(22) Kaneko, Y.; Nakano, M.; Sorai, M.; Jang, H. G.; Hendrickson, D. N. *Inorg. Chem.* **1989**, *28*, 1067.
(23) Dong, T.-Y.; Lee, T. Y.; Lin, H. M. *J. Organomet. Chem.* **1992**, *427*, 101.
(24) Dong, T.-Y.; Chang, C. K.; Huang, C. H.; Wen, Y. S.; Lee, S. L.; Chen, J. A.; Yeh, W. Y.; Yeh, A. *J. Chem. Soc., Chem. Commun.* **1992**, 526.
(25) Iijima, S.; Saida, R.; Motoyama, I.; Sano, H. *Bull. Chem. Soc. Jpn.* **1981**, *54*, 1375.

Table I. Extended Hückel Coulomb Integrals (H_{ii}) and Slater Exponents

	H_{ii} (eV)	ζ_1	ζ_2	c_1	c_2
C_{2s}	−21.4	1.625			
C_{2p}	−11.4	1.625			
H_{1s}	−13.6	1.300			
Fe_{3d}	−12.6	5.350	2.000	0.5505	0.6260
Fe_{4s}	−9.1	1.900			
Fe_{4p}	−5.32	1.900			

Table II. Experimental and Crystal Data for the X-ray Structures

	19	**20**	**22**
formula	$C_{28}H_{34}Fe_2$	$C_{28}H_{34}Fe_2$	$C_{28}H_{34}Fe_2I_3$
M_W	482.27	482.27	862.98
cryst syst	monoclinic	triclinic	triclinic
space group	$C2/c$	$P\bar{1}$	$P\bar{1}$
a, Å	18.760(3)	5.8649(6)	8.4567(20)
b, Å	9.568(3)	8.8462(6)	9.0268(15)
c, Å	16.441(3)	12.4822(11)	10.9182(12)
α, deg		109.814(6)	105.777(12)
β, deg	130.494(13)	103.063(8)	101.606(13)
γ, deg		83.476(6)	106.301(15)
ρ_{calcd}, g cm^{-3}	1.427	1.350	1.952
V, Å^2	2244.2(9)	539.01(9)	734.26(23)
Z	4	1	1
μ, mm^{-1}	1.30	1.23	4.12
λ, Å	0.70930	0.70930	0.70930
2θ limits, deg	49.8	54.8	44.9
max, min trans coeff	0.998, 0.901	0.998, 0.901	1.000, 0.609
R_f	0.038	0.046	0.042
R_{wf}	0.041	0.055	0.042

Table III. Atom Coordinates and Thermal Parameters (Å^2) for **19**

	x	y	z	Biso[a]
Fe	0.39766(4)	0.18619(6)	0.02633(5)	2.26(4)
C1	0.2775(3)	0.1897(5)	0.0077(3)	2.5(3)
C2	0.2638(3)	0.1102(5)	−0.0749(4)	3.1(3)
C3	0.3303(4)	−0.0014(5)	−0.0261(5)	3.7(4)
C4	0.3847(4)	0.0091(5)	0.0851(5)	3.6(4)
C5	0.3539(3)	0.1261(5)	0.1066(4)	3.0(3)
C6	0.4284(3)	0.3895(4)	0.0154(3)	2.5(3)
C7	0.4143(3)	0.3036(5)	−0.0645(3)	2.5(3)
C8	0.4803(3)	0.1934(5)	−0.0132(4)	2.7(3)
C9	0.5353(3)	0.2089(5)	0.0983(4)	3.0(3)
C10	0.5035(3)	0.3296(5)	0.1171(4)	2.9(3)
C11	0.3762(3)	0.5215(5)	−0.0050(4)	3.2(3)
C12	0.4020(5)	0.5923(7)	0.0933(6)	4.4(5)
C13	0.3439(4)	0.3326(6)	−0.1835(4)	3.5(3)
C14	0.3276(5)	0.2110(7)	−0.2519(5)	5.3(5)
H2	0.221(3)	0.131(5)	−0.150(4)	5.1(14)
H3	0.340(3)	−0.064(4)	−0.061(3)	3.1(10)
H4	0.430(4)	−0.047(5)	0.133(4)	5.3(14)
H5	0.372(3)	0.159(4)	0.168(3)	2.7(12)
H8	0.485(3)	0.124(4)	−0.046(3)	1.9(9)
H9	0.582(3)	0.137(5)	0.148(4)	4.4(12)
H10	0.523(3)	0.370(4)	0.184(3)	2.9(10)
H11-1	0.392(3)	0.588(5)	−0.042(4)	4.4(12)
H11-2	0.313(3)	0.500(5)	−0.051(4)	3.7(11)
H12-1	0.470(4)	0.624(5)	0.145(4)	5.3(13)
H12-2	0.396(4)	0.529(6)	0.136(4)	6.2(16)
H12-3	0.371(4)	0.674(6)	0.077(4)	5.5(14)
H13-1	0.366(2)	0.415(4)	−0.198(3)	1.3(8)
H13-2	0.289(3)	0.366(4)	−0.197(3)	3.1(10)
H14-1	0.388(4)	0.182(6)	−0.241(5)	8.8(19)
H14-2	0.286(4)	0.230(5)	−0.327(4)	5.5(14)
H14-3	0.305(4)	0.135(6)	−0.243(4)	5.4(16)

[a] Biso is the mean of the principal axes of the thermal ellipsoid.

third bands are **24** (9%) and **23** (35%), respectively. The second band was uncharacterized. The physical properties of **23** are as follows. ^{1}H NMR ($CDCl_3$, ppm): 1.17 (t, 6H, $-CH_3$), 2.37 (s, 3H, $-COCH_3$), 2.61 (m, 4H, $-CH_2-$), 3.99 (t, 2H, Cp), 4.03 (t, 2H, Cp), 4.19 (t, 1H, Cp), 4.48 (t, 1H, Cp). Mass spectrum: M^+ at m/z 335.

1,2,4-Triethyl-1′-bromoferrocene (25). Reduction of **23** with $LiAlH_4$/$AlCl_3$ in ether was carried out in a manner similar to the reduction of **15** and **16**. ^{1}H NMR ($CDCl_3$, ppm): 1.27 (t, 9H, $-CH_3$), 2.31 (m, 6H, $-CH_2-$), 3.88 (dd, 2H, Cp), 3.94 (s, 2H, Cp), 4.08 (dd, 2H, Cp). Mass spectrum: M^+ at m/z 348.

Table IV. Selected Bond Distances (Å) and Bond Angles (deg)

	19	**20**	**22**
	Distance		
Fe–C(1)	2.069(4)	2.069(3)	2.108(12)
Fe–C(2)	2.044(4)	2.044(4)	2.054(13)
Fe–C(3)	2.037(5)	2.045(4)	2.052(13)
Fe–C(4)	2.042(5)	2.040(4)	2.044(12)
Fe–C(5)	2.038(5)	2.047(4)	2.060(12)
Fe–C(6)	2.069(4)	2.057(4)	2.110(13)
Fe–C(7)	2.049(4)	2.043(4)	2.033(12)
Fe–C(8)	2.035(4)	2.052(4)	2.064(14)
Fe–C(9)	2.036(4)	2.041(4)	2.054(14)
Fe–C(10)	2.050(4)	2.034(4)	2.058(14)
C(1)–C(1)[a]	1.455(8)	1.456(7)	1.422(23)
C(1)–C(2)	1.427(6)	1.429(6)	1.396(18)
C(1)–C(5)	1.430(6)	1.431(5)	1.459(18)
C(2)–C(3)	1.429(7)	1.416(6)	1.434(21)
C(3)–C(4)	1.405(9)	1.409(7)	1.439(22)
C(4)–C(5)	1.406(7)	1.415(6)	1.385(20)
C(6)–C(7)	1.422(6)	1.418(6)	1.430(20)
C(6)–C(10)	1.431(6)	1.421(7)	1.430(22)
C(7)–C(8)	1.414(6)	1.420(7)	1.410(22)
C(8)–C(9)	1.410(7)	1.421(7)	1.422(24)
C(9)–C(10)	1.423(7)	1.401(7)	1.385(25)
I(1)–I(2)			2.9135(13)
	Angle		
C(2)–C(1)–C(5)	106.5(4)	106.6(3)	106.9(11)
C(1)–C(2)–C(3)	108.2(5)	108.6(4)	109.1(12)
C(2)–C(3)–C(4)	108.0(5)	108.0(4)	106.9(12)
C(3)–C(4)–C(5)	108.3(5)	108.4(4)	108.4(12)
C(1)–C(5)–C(4)	109.0(5)	108.4(4)	108.6(12)
C(7)–C(6)–C(10)	107.4(4)	106.5(4)	106.5(13)
C(6)–C(7)–C(8)	108.3(4)	109.2(4)	108.5(12)
C(7)–C(8)–C(9)	108.4(4)	106.8(4)	107.1(13)
C(8)–C(9)–C(10)	108.2(4)	108.4(4)	109.1(13)
C(6)–C(10)–C(9)	107.7(4)	109.0(4)	108.5(13)
I(2)–I(1)–I(2)[b]			180.0

[a] Symmetry equivalents: 0.5 − x, 0.5 − y, −z for **19**; −x, −y, −z for **20**; 1.0 − x, 1.0 − y, 1.0 − z for **22**. [b] Symmetry equivalents: −x, −y, −z.

1′,2′,4′,1‴,2‴,4‴-Hexaethylbiferrocene (26). The coupling reaction of **25** with activated Cu was carried out according to the procedure for the coupling of **17** and **18**. ^{1}H NMR ($CDCl_3$, ppm): 1.02 (t, 18H, $-CH_3$), 2.08 (q, 12H, $-CH_2-$), 3.69 (s, 4H, Cp), 3.93 (d, 4H, Cp), 4.01 (d, 4H, Cp). Mp: 40.8–41.5 °C. Mass spectrum: M^+ at m/z 538.

Mixed-Valence Compounds 2, 21, 22, and 27. Crystalline samples of these mixed-valence compounds were prepared (method 1) by adding a benzene/hexane (1:1) solution containing a stoichiometric amount of iodine to a benzene/hexane (1:1) solution of the corresponding biferrocene at 0 °C. The resulting dark green crystals were filtered and washed repeatedly with cold hexane. A more crystalline sample can be prepared by slowly diffusing hexane into a CH_2Cl_2 solution containing the corresponding biferrocenium triiodide salt (method 2). Microanalyses of the two different preparations were identical within experimental error. Anal. Calcd for the microcrystalline sample (method 1) of **2** ($C_{24}H_{26}Fe_2I_3$): C, 35.72; H, 3.00. Found: C, 35.48; H, 3.01. For a sample prepared by method 2, we found: C, 35.59; H, 3.02. Anal. Calcd for the microcrystalline sample (method 1) of **21** ($C_{28}H_{34}Fe_2I_3$): C, 38.97; H, 3.97. Found: C, 38.70; H, 3.83. For a method 2 sample of **21**, we found: C, 38.77; H, 3.88. Anal. Calcd for the microcrystalline sample (method 1) of **22** ($C_{28}H_{34}Fe_2I_3$): C, 38.97; H, 3.97. Found: C, 38.77; H, 3.01. For a method 2 sample of **22** we found: C, 38.98; H, 3.83. Anal. Calcd for the sample (method 1) of **27** ($C_{32}H_{42}Fe_2I_3$): C, 41.82; H, 4.61. Found: C, 41.00; H, 4.29. For a sample (method 2) of **27**, we found: C, 41.09; H, 4.28.

Physical Methods. ^{57}Fe Mössbauer measurements were made on a constant-velocity instrument which has been previously described.[16] The absolute temperature accuracy is estimated to be ±5 K, while the relative precision is ±0.5 K. Computer fittings of the ^{57}Fe Mössbauer data to Lorentzian lines were carried out with a modified version of a previously reported program.[26] Velocity calibrations were made using a 99.99%

(26) Lee, J. F.; Lee, M. D.; Tseng, P. K. *Chemistry* **1987**, *45*, 50.

Table V. Atom Coordinates and Thermal Parameters (Å²) for 20

	x	y	z	Biso[a]
Fe	0.08606(10)	0.06774(7)	0.22297(5)	3.244(23)
C1	−0.0200(7)	0.0640(4)	0.0524(3)	3.28(16)
C2	0.1281(7)	0.1950(5)	0.1198(3)	3.73(19)
C3	0.0219(8)	0.2948(5)	0.2121(4)	4.26(21)
C4	−0.1891(7)	0.2262(5)	0.2044(4)	4.22(20)
C5	−0.2163(7)	0.0844(5)	0.1069(3)	3.73(18)
C6	0.2660(8)	−0.1463(5)	0.2215(4)	4.04(20)
C7	0.4078(7)	−0.0143(5)	0.2901(4)	4.13(20)
C8	0.2976(9)	0.0846(5)	0.3816(4)	4.70(22)
C9	0.0844(9)	0.0123(6)	0.3688(4)	4.97(24)
C10	0.0652(8)	−0.1270(6)	0.2714(4)	4.77(24)
C11	0.3256(10)	−0.2821(6)	0.1200(4)	6.2(3)
C12	0.4322(18)	−0.4231(8)	0.1504(7)	11.7(6)
C13	0.4033(13)	0.2328(7)	0.4772(5)	8.5(4)
C14	0.2396(20)	0.3458(10)	0.5333(7)	13.3(7)
H2	0.278	0.210	0.097	4.9
H3	0.096	0.392	0.275	5.4
H4	−0.295	0.274	0.263	3.2
H5	−0.351	0.010	0.076	3.0
H7	0.562	0.017	0.281	5.6
H9	−0.040	0.060	0.416	5.4
H10	−0.060	−0.209	0.241	7.7
H11-1	0.430	−0.246	0.083	6.9
H11-2	0.169	−0.321	0.068	6.9
H12-1	0.576	−0.381	0.209	10.1
H12-2	0.480	−0.511	0.084	10.1
H12-3	0.333	−0.468	0.184	10.1
H13-1	0.499	0.294	0.443	7.5
H13-2	0.500	0.192	0.539	7.5
H14-1	0.133	0.273	0.545	10.5
H14-2	0.153	0.405	0.483	10.5
H14-3	0.312	0.421	0.608	10.5

[a] Biso is the mean of the principal axes of the thermal ellipsoid.

pure 10-μm iron foil. Typical line widths for all three pairs of iron lines fell in the range 0.24–0.27 mm s^{-1}. Isomer shifts are reported relative to iron foil at 300 K but are uncorrected for temperature-dependent, second-order Doppler effects. It should be noted that the isomer shifts illustrated in the figures are plotted as experimentally obtained. Tabulated data is provided.

^{1}H NMR spectra were run on a Bruker MSL200 spectrometer. Mass spectra were obtained with a VG250-70S system. Electron paramagnetic resonance data (X-band) were collected with a Bruker ER200D-SRC spectrometer. The magnetic field was calibrated with a Bruker ER035M NMR gaussmeter. DPPH was used to gauge the microwave frequency. A direct-immersion dewar, which was inserted into the cavity, was use to obtain 77-K data.

Electrochemical measurements were carried out with a BAS 100B system. Cyclic voltammetry was performed with a stationary glassy carbon working electrode, which was cleaned after each run. These experiments were carried out with 1×10^{-3} M solutions of biferrocene in dry CH_2Cl_2/CH_3CN (1:1) containing 0.1 M of $(n\text{-}C_4H_9)_4NPF_6$ as supporting electrolyte. The potentials quoted in this work are relative to a Ag/AgCl electrode at 25 °C. Under these conditions, ferrocene shows a reversible one-electron oxidation wave ($E_{1/2}$ = 0.38 V).

Theoretical Calculations. Theoretical calculations of the fragment orbitals for bending of biferrocenium triiodide (1) from parallel geometry to a structure with a tilt angle of up to 60° were performed by using the semiempirical extended Hückel method.[27] Correlation between the HOMO–LUMO gap and the tilt angle was also made. The atomic parameters used in the calculations were taken from ref 13 and are listed in Table I.

Structure Determination of 19. An orange crystal (0.21 × 0.25 × 0.41 mm), which was grown by slow evaporation from a hexane solution, was used for data collection at 298 K. Cell dimensions (obtained from 25 reflections with 19.42° < 2θ < 34.70°) and space group data were obtained by standard methods on an Enraf Nonius CAD4 diffractometer. The θ–2θ scan technique was used to record the intensities for all reflections for which 1° < 2θ < 49.8°. Absorption corrections were made with empirical Ψ rotation. Of the 1974 unique reflections, there were 1405 with $F_o > 2.0\sigma(F_o^2)$, where $\sigma(F_o^2)$ values were estimated from counting statistics. These data were used in the final refinement of the structural parameters. The X-ray crystal data are summarized in Table II.

(27) Lauher, J. W.; Hoffmann, R. *J. Am. Chem. Soc.* **1976**, *98*, 1729.

Table VI. Atom Coordinates and Thermal Parameters (Å²) for 22

	x	y	z	Biso[a]
I1	0.00000	0.00000	0.00000	5.37(10)
I2	0.10932(16)	−0.03319(15)	0.25872(13)	7.40(9)
Fe	0.33915(24)	0.58880(23)	0.82438(19)	3.39(11)
C1	0.4472(16)	0.5489(15)	0.9987(12)	3.1(8)
C2	0.5016(18)	0.7160(16)	1.0155(13)	3.7(8)
C3	0.3536(21)	0.7646(17)	0.9955(13)	4.5(9)
C4	0.2039(19)	0.6188(20)	0.9590(13)	4.5(10)
C5	0.2588(17)	0.4881(17)	0.9593(12)	3.7(8)
C6	0.4125(20)	0.4773(17)	0.6595(13)	4.1(9)
C7	0.4592(17)	0.6515(17)	0.6925(13)	4.0(9)
C8	0.3070(22)	0.6890(21)	0.6764(15)	4.9(10)
C9	0.1669(19)	0.5395(23)	0.6436(14)	5.1(10)
C10	0.2299(21)	0.4123(19)	0.6364(13)	5.0(10)
C11	0.5306(22)	0.3783(19)	0.6591(14)	5.3(10)
C12	0.7141(22)	0.4789(22)	0.7022(16)	6.9(13)
C13	0.2960(28)	0.8576(26)	0.6978(18)	9.1(16)
C14	0.2799(30)	0.9060(23)	0.5885(24)	10.6(17)
H2	0.592	0.811	1.009	6.3
H3	0.371	0.884	1.012	6.3
H4	0.128	0.687	0.967	6.3
H5	0.173	0.376	0.947	6.3
H7	0.583	0.717	0.702	6.3
H9	0.058	0.560	0.653	6.3
H10	0.184	0.307	0.655	6.3
H11-1	0.522	0.337	0.734	6.3
H11-2	0.503	0.295	0.569	6.3
H12-1	0.784	0.408	0.691	6.3
H12-2	0.747	0.544	0.798	6.3
H12-3	0.725	0.550	0.647	6.3
H13-1	0.406	0.943	0.771	6.3
H13-2	0.200	0.869	0.735	6.3
H14-1	0.296	0.816	0.520	6.3
H14-2	0.382	1.007	0.610	6.3
H14-3	0.169	0.918	0.561	6.3

[a] Biso is the mean of the principal axes of the thermal ellipsoid.

A three-dimensional Patterson synthesis was used to determine the heavy-atom positions, which phased the data sufficiently well to permit location of the remaining non-hydrogen atoms from Fourier synthesis. All non-hydrogen atoms were refined anisotropically. During the final cycles of refinement, fixed hydrogen contributions with C–H bond lengths fixed at 1.08 Å were applied. The final positional parameters for all atoms can be found in Table III, and the selected bond distances and angles are given in Table IV. Listings of the thermal parameters and observed and calculated structure factors are given as supplementary materials.

Structure Determination of 20. A needlelike crystal (0.20 × 0.16 × 0.44 mm) was obtained by following the same procedure as described for **19**. Data were collected to a 2θ value of 54.8°. Absorption corrections were also made. The unit cell dimensions were obtained from 25 reflections with 15.09° < 2θ < 34.03°. Of the 2724 unique reflections, there were 2020 with $F_o > 2.0\sigma(F_o^2)$. These data were used in the final refinement of structural parameters. The structure was solved by the heavy-atom method to locate the Fe positions and successive Fourier maps to reveal the whole molecule and refined with a weighted least-squares routine. The unit cell parameters are given in Table II. Atomic coordinates and selected bond distances and angles are given in Tables V and IV, respectively. Listing of the thermal parameters and observed and calculated structure factors are available as supplementary materials.

Structure Determination of 22. A dark black crystal (0.22 × 0.22 × 0.01 mm) was obtained when a layer of hexane was allowed to slowly diffuse into a CH_2Cl_2 solution of **22**. Data were collected to a 2θ value of 44.9°. The cell dimensions were obtained from 25 reflections with 2θ in the range 15.53–31.90°. The data were also corrected for absorption with an empirical Ψ rotation. Of the 1914 unique reflections, there were 999 with $F_o^2 > 2.0\sigma(F_o^2)$. These data were used in the final refinement of the structural parameters. Details of data collection and unit cell parameters are given in Table II.

Structure refinement was carried out in the same manner as described for **19**. The greatest residual electron density upon completion of refinement was in the vicinity of the iodide atoms. Atomic coordinates are given in Table IV. Listings of the thermal parameters and observed and calculated structure factors are available as supplementary materials.

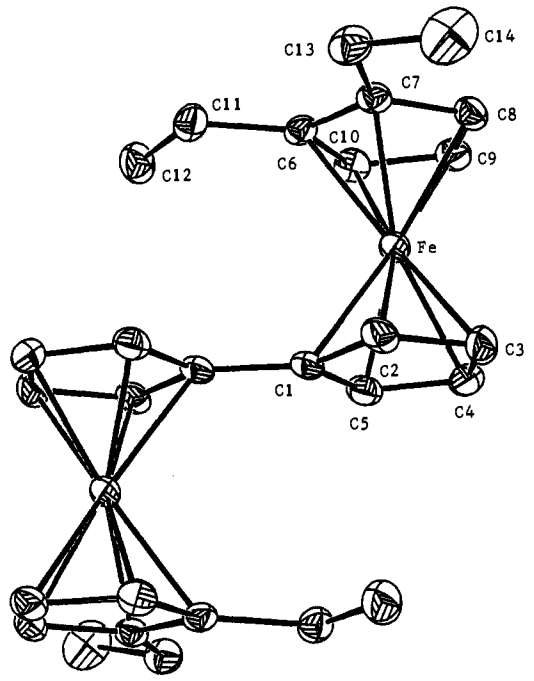

Figure 1. ORTEP drawing for **19** with 30% thermal ellipsoids.

Results and Discussion

Although the physical properties of **19** and **20** are different, it is difficult to assign their structures with certainty solely with NMR spectroscopy. X-ray crystallographic studies of these complexes were undertaken to help us to elucidate the geometric influences on the rate of intramolecular electron transfer in mixed-valence biferrocenium cations. Before the new physical data are described, a summary of single-crystal X-ray structural results obtained for **19**, **20**, and **22** will be presented.

Molecular Structure of 19. The results of our crystallographic study at room temperature show that **19** crystallizes in the monoclinic space group $C2/c$. The structure imposed an inversion center on the biferrocene molecule. The molecule exists in a trans conformation with the two iron ions on opposite sides of the planar fulvalenide ligand. An ORTEP drawing of the molecule is shown in Figure 1, and selected bond distances and angles are given in Table IV. Inspection of the iron to Cp ligand bond lengths (Fe–Cp) shows that both distances (1.652(3) and 1.653(3) Å) are closer to the value of 1.65 Å found[28] for ferrocene than to the value of 1.70 Å found[29] for the ferrocenium ion. The dihedral angle between the least-squares planes of the Cp rings is 2.0(3)°, while the two Cp rings bonded to each iron ion are nearly eclipsed with an average staggering angle of 1.9(1)°. The average Fe–C bond distance of 2.047(4) Å is also closer to the value of 2.045 Å found for neutral ferrocene than to the value of 2.075 Å found for the ferrocenium cation. The average C–C bond length (1.420(8) Å) in the rings agrees well with that in ferrocene (1.42 Å).

Molecular Structure of 20. Compound **20** crystallizes at room temperature in the triclinic space group $P\bar{1}$. As shown in Figure 2, the molecule adopts the usual trans conformation seen in other dialkyl analogies. Collected in Table IV are selected bond distances and angles. A direct comparison was made between **19** and **20** (Table VII). The average bond distance between the iron atom and the five carbons of a given ring and the average Fe–Cp distance for a ferrocene moiety are very similar in both compounds **19** and **20**. The plane of the Cp ring forms a dihedral angle of 1.07(2)° with the fulvalenide plane, and the two Cp rings in each ferrocenyl moiety are nearly eclipsed with an average staggering angle of 1.6(1)°. The average C–C bond length (1.418(6) Å) in the rings also agrees well with that in ferrocene (1.42 Å).

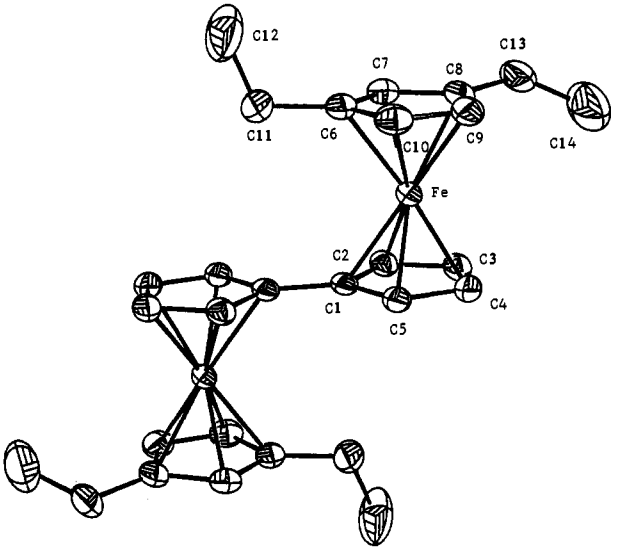

Figure 2. ORTEP drawing for **20** with 30% thermal ellipsoids.

Table VII. Comparison of the Atomic Distances (Å) and Angles (deg)

compound	Fe–C	Fe–Cp	tilt angle	stagger angle	T_c (K)[a]
biferrocene	2.052(3)	1.64(2)	1.2	16	
1′,1‴-diethyl-biferrocene	2.07(1)	1.66(4)	2.3	3.6	
19	2.047(4)	1.652(3)	2.0(3)	1.9(1)	
20	2.047(4)	1.654(2)	1.07(2)	1.6(1)	
1	2.060(6)	1.68(4)	0.3(3)	0.0	~365
2	2.06(1)	1.676(5)	4.8		275
3	2.06(1)	1.677(9)	6.6	1.2	245
22	2.06(1)	1.672(8)	5.9(7)	3.6(1)	125
11	2.072(5)	1.674	15.6		<4.2
7	2.063(3)	1.672(1)	3.3(4)	1.2(1)	190
5	2.070	1.678	2.3	6.6	110
10	2.063(8)	1.673(2)	4.7(3)	2.32(5)	<77

[a] Temperature for the localization–delocalization transition on Mössbauer technique.

Molecular Structure of 22. Compound **22** crystallizes in the triclinic space group $P\bar{1}$. Figure 3 shows the molecular structure and atomic labeling scheme for the cation and anion. Atomic coordinates and important metrical parameters are given in Table VI and IV, respectively. Compound **22** has the usual trans conformation seen in other dialkyl mixed-valence biferrocenium triiodide salts. A comparison of **22** with the series of biferrocenium salts was also made (Table VII). Mean bond distance between the iron atom and the five carbon atoms of a given ring is 2.06(1) Å, which is larger than that for the neutral compound **20**. It also lies midway between the 2.045 Å observed[28] for ferrocene and 2.075 Å observed[29] for the ferrocenium cation. The average Fe–Cp bond length is 1.672(8) Å, which is also larger than that for the corresponding neutral biferrocene **20**. Such an increase in Fe–C and Fe–Cp distances has been observed when ferrocenes are oxidized to the corresponding ferrocenium cations.[16] There is no significant difference for C–C bond distances in the rings between **20** (1.418(6) Å) and **22** (1.42(2) Å). The dihedral angle between the least-squares planes of the Cp rings is 5.9(7)°, while the two Cp rings in each ferrocenyl moiety are nearly eclipsed with an average staggering angle of 3.6(1)°. The site symmetry imposed on the mixed-valence cation obviously requires that both iron centers of the cation are in equivalent positions in the unit cell, and this is consistent with our Mössbauer studies. Fur-

(28) Seiler, P.; Dunitz, J. D. *Acta Crystallogr., Sect. B* **1979**, *35*, 1068.
(29) Mammano, N. J.; Zalkin, A.; Landers, A.; Rheingold, A. L. *Inorg. Chem.* **1977**, *16*, 297.

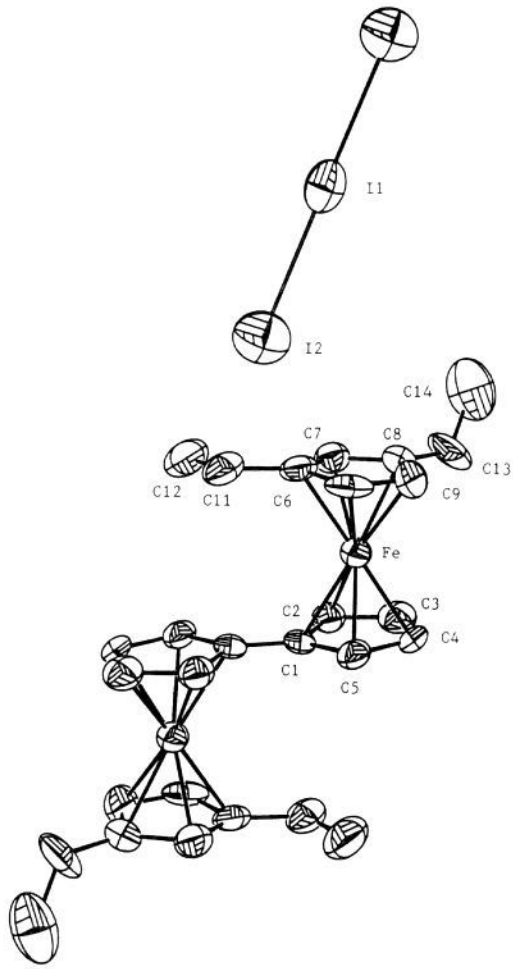

Figure 3. ORTEP drawing for **22** with 50% thermal ellipsoids.

thermore, an analysis of the thermal parameters of the ring carbon atoms indicates that this is not the result of a disordered localized structure.

The I_3^- anion is also at the inversion center, showing a symmetric structure. The I–I bond distance is 2.914(1) Å, which is in accord with the accepted value of 2.92 Å reported for the free I_3^- ion.[30]

An interesting finding is that the two ethyl substituents on the Cp ring are situated differently. The ethyl group located at the position above the ring of the other sandwich is parallel to the fulvalenide plane, and this is in contrast to the compound **2**, in which the ethyl group is not parallel to the fulvalenide moiety but stands perpendicular to the fulvalenide ligand.[31] In the case of **3**, the propyl group is also parallel to the fulvalenide plane.[32] The carbon atom framework of the other ethyl group on the Cp ring in **22** runs essentially perpendicular to the fulvalenide ligand. Consequently, the packing arrangement of the cations and anions in **22** is different from those in **1–3** (Figure **4**). In the case of **1**[9] and **3**,[32] the packing arrangement can be described as steplike columns. As shown in Figure 5, the packing arrangement in **22** can be described as columns of cations and anions developing approximately along the *c* axis, where each column of cations is surrounded by four columns of the anions. Furthermore, it appears that the perpendicular ethyl group on the Cp ring in **22** leads to further slippage of the cations from the steplike stacks seen in **1** and **3**. As shown in Figure 6, there is no Cp–Cp overlap between neighboring cations in the solid-state structure of **22**. In the case of **3**, the Cp–Cp interplanar distance is ~3.5 Å and an intermolecular $\pi-\pi$ interaction is expected between neighboring cations.

Three-dimensional hydrogen bonding is clearly found between the cyclopentadienyl hydrogen atoms and the iodine atoms. The closest contact between cations and anions is I(2)–H(7) (3.134-

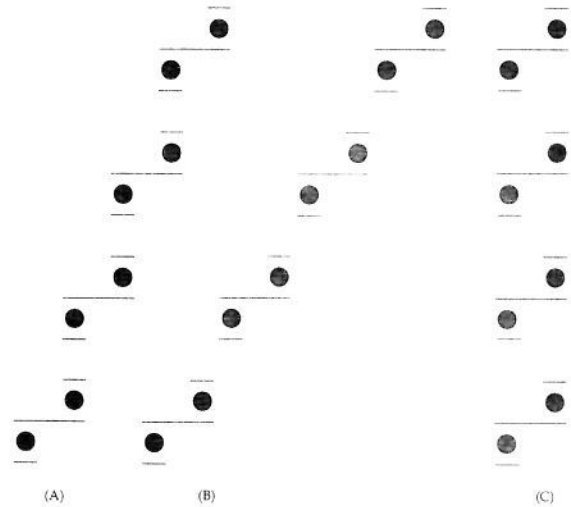

Figure 4. Stacking models for (A) **1** and **3**, (B) **2**, and (C) **22**.

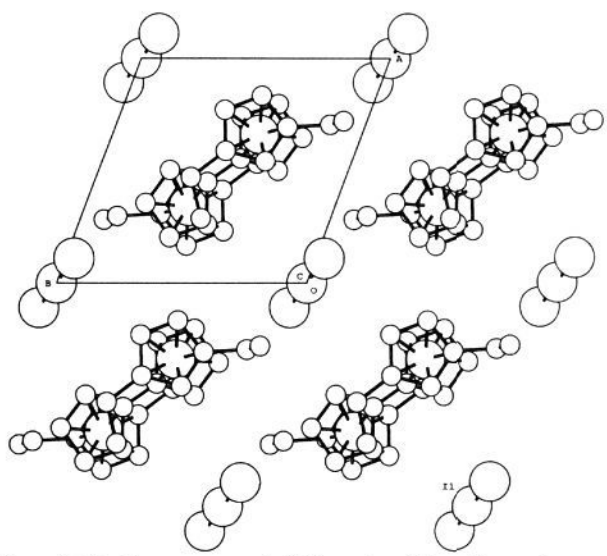

Figure 5. Packing arrangement of **22** as viewed down the *c* axis.

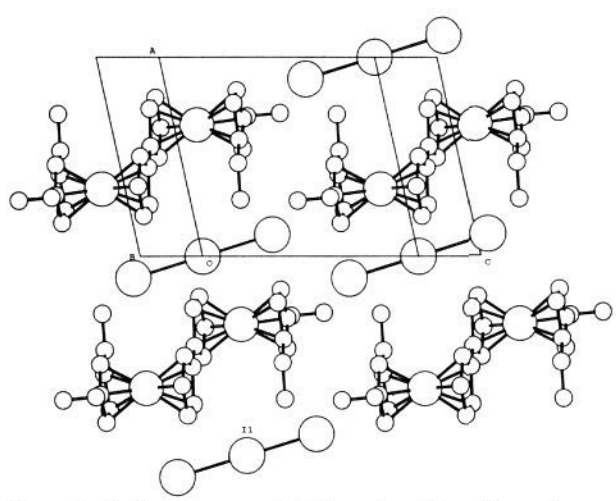

Figure 6. Packing arrangement of **22** as viewed down the *x* axis.

(30) Runsink, J.; Swen-Walstra, S.; Migchelsen, T. *Acta Crystallogr., Sect. B* **1972**, *28*, 1331.
(31) Michiko, K.; Sano, H. *Bull. Chem. Soc. Jpn.* **1988**, *61*, 1455.
(32) Michiko, K.; Sano, H.; Iijima, S. *Bull. Chem. Soc. Jpn.* **1982**, *55*, 2327.

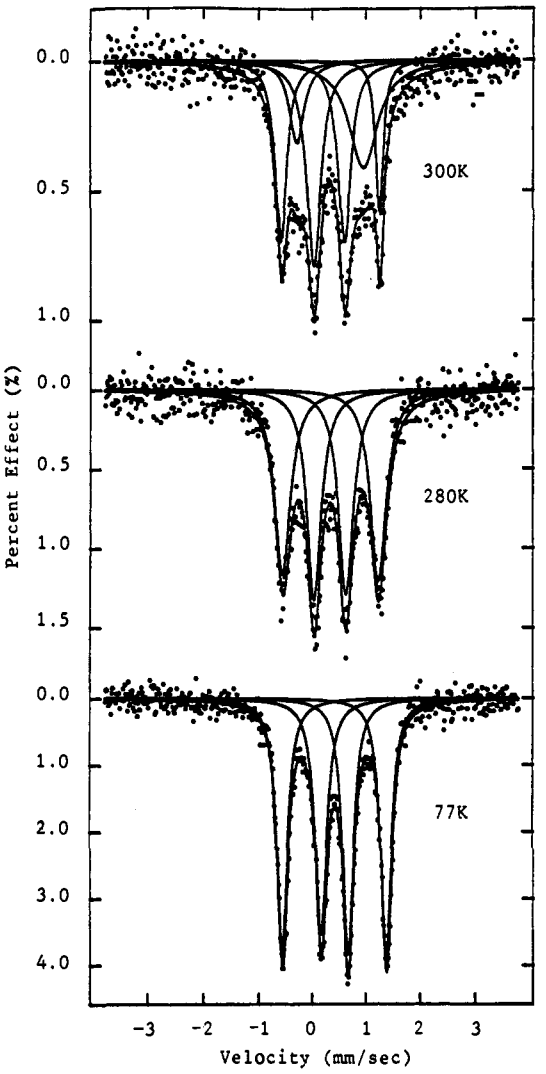

Figure 7. ^{57}Mössbauer spectra of **2** prepared by method 1.

(1) Å). There is also a hydrogen bond network (3.348(2) Å) between perpendicular ethyl groups and I_3^- anions. We believe that the hydrogen bond networks between the alkyl substituents and the I_3^- anions in the series of mixed-valence biferrocenium salts play an important role in determining the degree of tilting of the Cp rings from parallel geometry. In turn, we believe that the tilting of the Cp rings has a pronounced influence on the rate of electron transfer. From Table VII, it can be easily seen that the decreases of the critical temperatures for the delocalization–localization transition (Mössbauer technique 10^7 s^{-1}) in the series of mixed-valence biferrocenium salts were accompanied by the increases of the tilting angle. In other words, there is a correlation between the tilt angle and the rate of electron transfer: the larger the tilt angle, the faster the electron transfer. A detailed discussion will be presented in the next section.

^{57}Fe Mössbauer Characteristics. It has been noted[9] that the ^{57}Fe Mössbauer spectral properties of **4** and **5** are dependent on sample history. To examine this phenomenon more thoroughly, we prepared samples of **2**, **21**, **22**, and **27** by two different methods as described in the Experimental Section. Firstly, we reconfirmed that a microcrystalline sample of **2**, formed by adding a benzene solution of iodine to a benzene solution of 1′,1‴-diethylbiferrocene, does exhibit two doublets at temperatures below 250 K.[9] Increasing the temperature causes the two doublets to move together with no discernible line broadening and eventually to become a single "average-valence" doublet at temperature 275 K. However, it was curious to find that the 300-K ^{57}Fe Mössbauer spectrum of the microcrystalline sample prepared by method 1 consists of valence-trapped and valence-detrapped signals. The

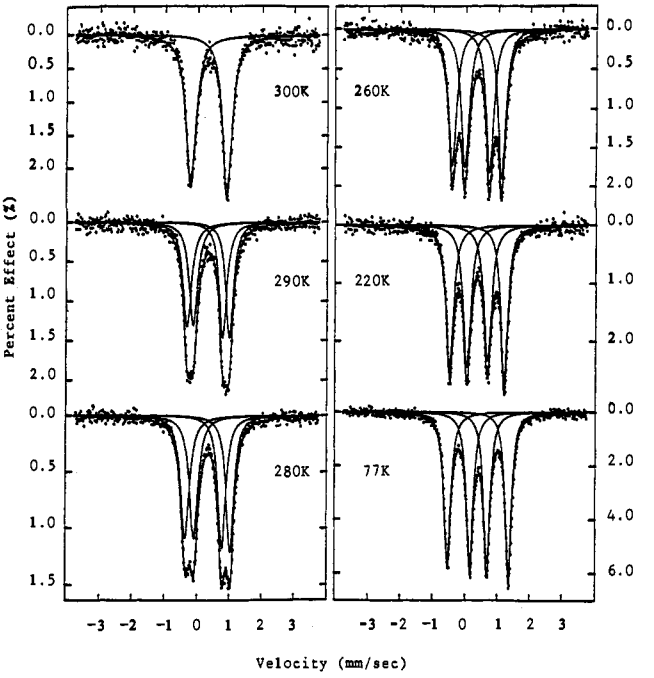

Figure 8. Variable-temperature ^{57}Mössbauer spectra of **2** prepared by method 2.

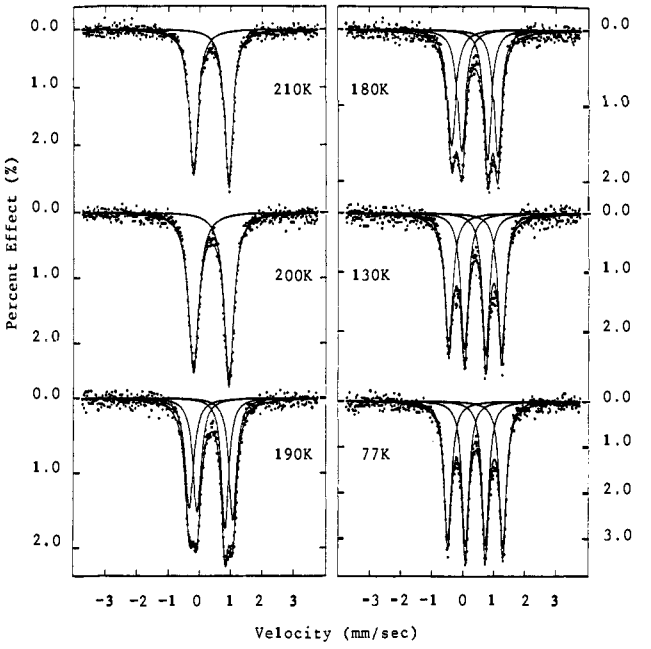

Figure 9. Variable-temperature ^{57}Mössbauer spectra of **21** prepared by method 1.

variable-temperature ^{57}Fe Mössbauer spectra of **2** (method 1) are shown in Figure 7. The various absorption peaks were fitted to Lorentzian lines. The resulting fitting parameters are collected in Table VIII. At 77 K, the Mössbauer spectrum shows two doublets, one for Fe(II) metallocene (ΔE_Q = 1.936 mm s^{-1}) and the other for Fe(III) metallocene (ΔE_Q = 0.479 mm s^{-1}). These two doublets do not coalesce into an "average-valence" doublet at 275 K as reported previously.[9] The prominent features in the 300-K Mössbauer spectrum are two doublets, one with a ΔE_Q = 1.829 mm s^{-1} (Fe(II) metallocene) and the other with ΔE_Q = 0.540 mm s^{-1} (Fe(III) metallocene). Both doublets have the same area. This pattern of two doublets is what is expected for a mixed-valence biferrocenium cation which is valence trapped on the Mössbauer time scale ($\sim 10^7$ s^{-1}). Fitting the 300-K spectrum also clearly shows a third doublet with ΔE_Q = 1.037 mm s^{-1}. This doublet is associated with a mixed-valence

Table VIII. ^{57}Fe Mössbauer Least-Squares-Fitting Parameters

compound	T (K)	ΔE_Q[a]	δ[b]	Γ[c]	compound	T (K)	ΔE_Q[a]	δ[b]	Γ[c]
2[d]	300	0.540	0.436	0.240, 0.242			1.866	0.486	0.274, 0.282
		1.037	0.440	0.637, 0.639		77	0.499	0.506	0.357, 0.329
		1.829	0.447	0.225, 0.232			1.118	0.489	0.506, 0.505
	280	0.587	0.442	0.332, 0.324			1.882	0.500	0.259, 0.263
		1.786	0.452	0.355, 0.369	**22**[d,f]	300	1.138	0.434	0.254, 0.256
	77	0.497	0.524	0.242, 0.262		150	1.187	0.495	0.347, 0.352
		1.936	0.520	0.235, 0.238		140	1.011	0.500	0.294, 0.282
2[e]	300	1.124	0.442	0.341, 0.367			1.365	0.499	0.277, 0.280
	290	0.922	0.443	0.281, 0.315		130	0.972	0.493	0.288, 0.318
		1.302	0.444	0.282, 0.312			1.410	0.496	0.281, 0.282
	280	0.866	0.451	0.290, 0.315		120	0.925	0.504	0.281, 0.277
		1.388	0.452	0.282, 0.314			1.440	0.506	0.282, 0.311
	260	0.752	0.459	0.284, 0.296		78	0.824	0.403	0.280, 0.276
		1.524	0.456	0.273, 0.299			1.572	0.399	0.276, 0.288
	220	0.630	0.477	0.290, 0.279	**22**[d,g]	300	1.136	0.430	0.277, 0.264
		1.681	0.475	0.252, 0.275		140	1.178	0.491	0.341, 0.348
	77	0.518	0.527	0.249, 0.252		130	1.178	0.500	0.366, 0.363
		1.883	0.521	0.226, 0.252		120	1.004	0.499	0.305, 0.300
21[d]	210	1.142	0.470	0.314, 0.342			1.353	0.498	0.307, 0.310
	200	1.147	0.475	0.365, 0.397		110	0.950	0.499	0.289, 0.324
	190	0.907	0.478	0.276, 0.316			1.420	0.497	0.323, 0.310
		1.405	0.479	0.294, 0.327		80	0.906	0.509	0.307, 0.314
	180	0.845	0.486	0.294, 0.314			1.492	0.505	0.314, 0.318
		1.490	0.484	0.300, 0.329	**22**[e]	300	1.140	0.436	0.259, 0.384
	130	0.696	0.498	0.279, 0.291		140	1.196	0.499	0.317, 0.343
		1.712	0.499	0.285, 0.308		130	1.203	0.503	0.363, 0.384
	77	0.651	0.512	0.271, 0.269		125	1.016	0.502	0.279, 0.301
		1.785	0.508	0.266, 0.282			1.383	0.503	0.287, 0.305
21[e]	300	0.345	0.421	0.258, 0.240		120	0.991	0.506	0.279, 0.301
		1.127	0.430	0.227, 0.241			1.415	0.502	0.287, 0.305
		1.911	0.422	0.244, 0.241		115	0.968	0.507	0.275, 0.302
	250	0.351	0.448	0.283, 0.264			1.446	0.505	0.281, 0.300
		1.136	0.452	0.242, 0.254		100	0.918	0.512	0.282, 0.297
		1.933	0.444	0.229, 0.226			1.510	0.509	0.284, 0.306
	220	0.350	0.457	0.292, 0.278		77	0.871	0.519	0.277, 0.300
		1.152	0.463	0.338, 0.362			1.570	0.512	0.272, 0.299
		1.935	0.458	0.230, 0.237	**27**[d]	300	2.039	0.406	0.286, 0.290
	180	0.548	0.476	0.472, 0.431			0.522	0.412	0.432, 0.395
		1.105	0.465	0.473, 0.472		77	2.031	0.405	0.283, 0.286
		1.800	0.468	0.330, 0.433			0.521	0.411	0.429, 0.392
	130	0.510	0.494	0.371, 0.360	**27**[e]	300	1.933	0.328	0.266, 0.301
		1.106	0.492	0.515, 0.476			0.516	0.330	0.360, 0.345

[a] Quadruple-splitting in mm s^{-1}. [b] Isomer shift referenced to iron foil in mm s^{-1}. [c] Full width at half-height taken from the least-squares-fitting program. The width for the line at more positive velocity is listed first for each doublet. [d] Prepared by method 1. [e] Prepared by method 2. [f] Nonground sample. [g] Ground sample.

biferrocenium cation in which the electron-transfer rate is greater than the Mössbauer time scale. The ratio of valence-localized to valence-delocalized species in the 300-K spectrum is 1.00:1.03. The crystalline sample prepared by method 2 gives a Mössbauer spectrum at 300 K that shows only a single average doublet. Figure 8 shows variable-temperature Mössbauer spectra obtained for a more crystalline sample (method 2). At 220 K and below, only two doublets can be seen, one characteristic of a Fe(II) metallocene and the other characteristic of a Fe(III) metallocene. Mössbauer fitting parameters are also summarized in Table VIII. As the temperature is increased, the two doublets move together to become a single doublet at ~295 K, but not 275 K as reported previously. Obviously, the intramolecular electron transfer in **2** is quite sensitive to environmental perturbations caused by different crystal packing arrangements.

Two different preparations of **21** were also examined with variable-temperature Mössbauer spectroscopy. Several unusual observations that have been made for **1**, **2**, **4**, and **5** have also been seen for this new mixed-valence compound **21**. Figure 9 illustrates the spectra obtained for a sample prepared by method 1. The two doublets are seen to move together as the sample temperature is increased, finally becoming a single average doublet at ~195 K. Thus, in comparison with **2**, the ethyl substituents on the Cp ring of **21** led to a reduction by ~80° in the temperature where the mixed-valence cation of **21** transfers an electron faster than the Mössbauer technique. On the other hand, the sample of **21** obtained by method 2 gives Mössbauer spectra with localized (two doublets) and delocalized (one average doublet) spectra superimposed (Figure 10). Collected in Table VIII are the resulting fitting parameters. Examination of the 77-K spectrum reveals that it consists of valence-trapped (Fe(II), ΔE_Q = 1.882 mm s^{-1}; Fe(III), ΔE_Q = 0.499 mm s^{-1}) and valence-detrapped (Fe(II/III), ΔE_Q = 1.118 mm s^{-1}) signals. As the temperature is increased, the intensity of the detrapped signal grows at the expense of trapped signal. The ratio of valence-localized to valence-delocalized species changes from 1:0.22 to 1:1.13 as the temperature is changed from 77 to 300 K.

^{57}Fe Mössbauer spectra for samples of **22** obtained by two different preparations were also collected at temperatures ranging from 77 to 300 K. Selected spectra are shown in Figures 11–13, and the fitting parameters are listed in Table VIII. An interesting finding for this particular new mixed-valence compound is that grinding the sample has a pronounced influence on the rate of intramolecular electron transfer. The ^{57}Fe Mössbauer spectra of a nonground sample of **22** prepared by method 1 at various temperatures are shown in Figure 11. At temperatures below 130 K, the cation of **22** shows two doublets in the variable-temperature Mössbauer spectra, one representing the Fe(II) site and the other for the Fe(III) site. An increase of temperature causes the two doublets to move together, resulting in an "average-valence" doublet at 145 K. Figure 12 illustrates the variable-temperature Mössbauer spectra for the manually ground sample of **22** obtained by method 1. At temperatures above 125 K, the spectrum of this sample shows a single quadrupole-split doublet

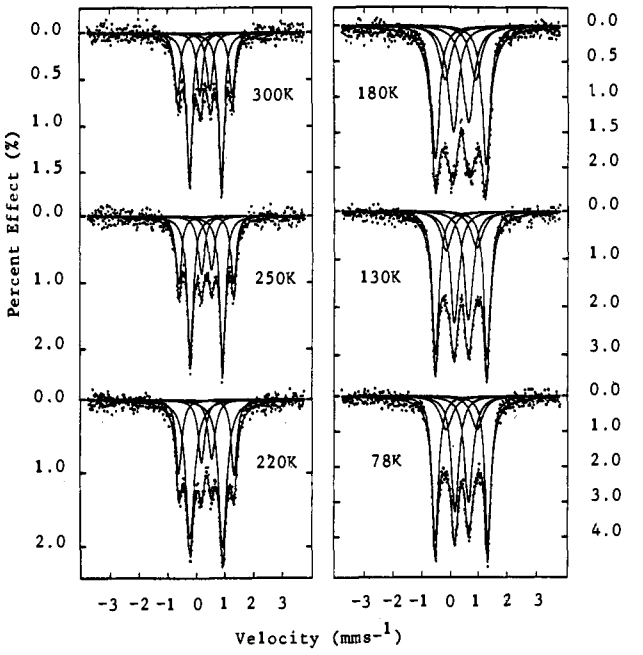

Figure 10. Variable-temperature ^{57}Mössbauer spectra of **21** prepared by method 2.

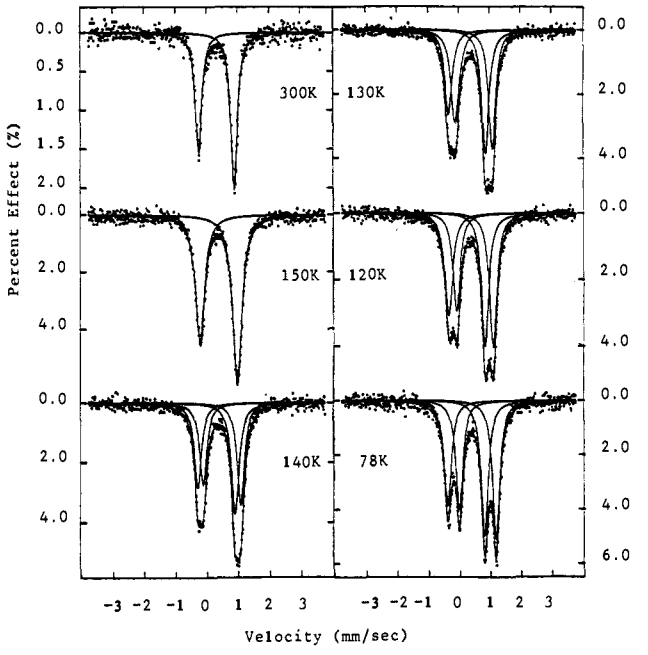

Figure 11. Variable-temperature ^{57}Mössbauer spectra for a nonground sample of **22** prepared by method 1.

which is characteristic of a valence-detrapped cation in which the electron-transfer rate exceeds $\sim 10^7\,s^{-1}$. Thus, there is an increase in the electron-transfer rate as a result of grinding the sample; this is in contrast to the observation made for **5**.[33] In the case of **5**, Hendrickson found a reduction of the electron-transfer rate as a result of mechanical grinding. Mechanical grinding is known to introduce a much higher concentration of defects. Hendrickson suggested that a cation of **5** situated close to a defect such as a dislocation would become trapped due to the introduction of a zero-point energy difference between the two vibronic descriptions of the cation.[33] In other words, this observation was interpreted in terms of a domain nucleation and growth model of phase transition. This model has also been well studied for spin–

(33) Webb, R. J.; Dong, T.-Y.; Pierpont, C. G.; Boone, S. R.; Chadha, R. K.; Hendrickson, D. N. *J. Am. Chem. Soc.* **1991**, *113*, 4806.
(34) Ritter, G.; König, E.; Irler, W.; Goodwin, H. A. *Inorg. Chem.* **1978**, *17*, 224.

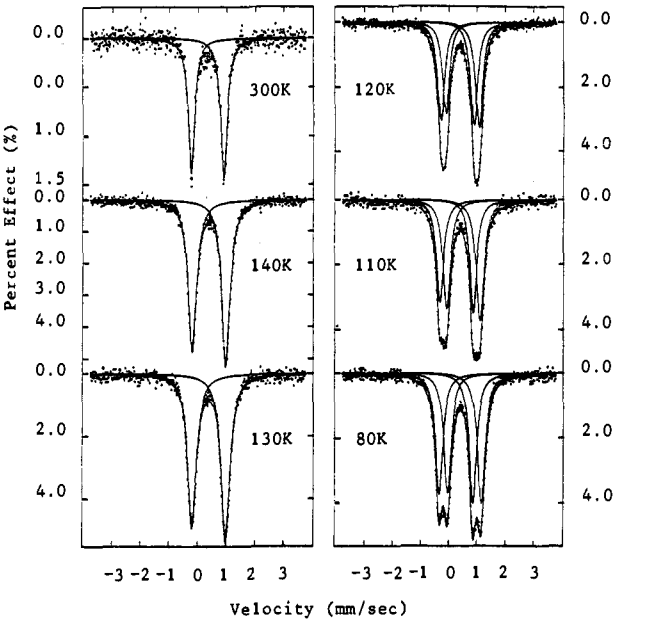

Figure 12. Variable-temperature ^{57}Mössbauer spectra for a ground sample of **22** prepared by method 1.

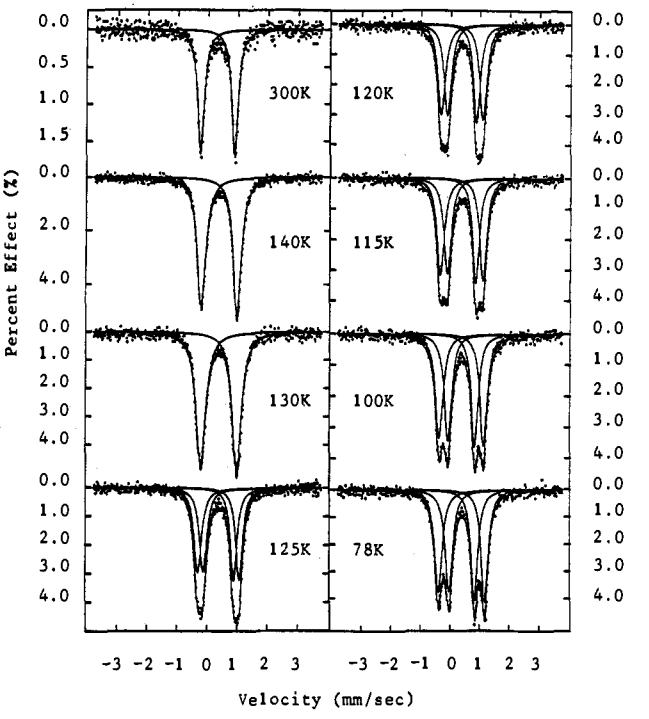

Figure 13. Variable-temperature ^{57}Mössbauer spectra of **22** prepared by method 2.

crossover transitions.[34] In this model, defects introduced by grinding create kinetic barriers to domain growth so that metastable domains possess insufficient time and thermal energy to effect a complete conversion. Additionally, defects certainly weaken the cooperative interaction between molecules. Obviously, our observation cannot be interpreted in terms of this model. It is possible that the manual grinding leads to a reduction of crystalline size, resulting in an increase of the electron-transfer rate.

The variable-temperature Mössbauer spectra of **22** obtained by method 2 are illustrated in Figure 13, and Mössbauer fitting parameters are also given in Table VIII. This sample gave essentially identical spectra in comparison with the ground sample prepared by method 1. The two valence-trapped doublets coalesce

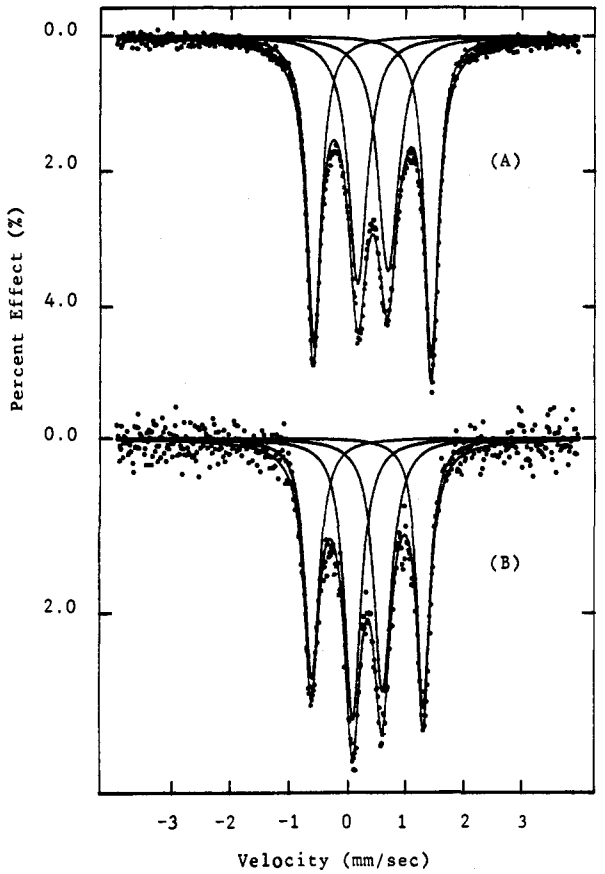

Figure 14. Variable-temperature ^{57}Mössbauer spectra at 300 K for **27** (A) prepared by method 1 and (B) prepared by method 2.

into a single valence-detrapped doublet at ~127 K as the temperature is increased.

The Mössbauer results indicate that compounds **21** and **22** are valence delocalized on the Mössbauer time scale in the solid state above 195 and 125 K, respectively. Thus, the change of the relative positions of the ethyl substituents from 1′,3′,1‴,3‴ in **22** to 1′,2′,1‴,2‴ in **21** leads to a reduction in the intramolecular electron-transfer rate and the ordering of intramolecular electron-transfer rates is **22** > **21** > **2** > **1**. We now propose a model to explain the difference in transition temperatures for delocalization in the mixed-valence cations **1**, **2**, **21**, and **22**. We believe that the difference in transition temperatures is not due only to a difference in the electronic effect of the ethyl substituents. The Mössbauer studies of 1′,2′,4′,1‴,2‴,4‴-hexaethylbiferrocenium triiodide (**27**) strongly support our suggestion. The 300-K Mössbauer spectra of **27** for the two different preparations are shown in Figure 14. Both samples gave essentially identical spectra. The features in the 300-K Mössbauer spectrum are two doublets (Fe(II), ΔE_Q = ~2.0 mm s^{-1}; Fe(III), ΔE_Q = ~0.52 mm s^{-1}). This pattern is expected for a mixed-valence cation which is valence trapped on the time scale of the Mössbauer technique (electron-transfer rate < ~10^7 s^{-1}). Hence, an extra ethyl substituent on the Cp ring of **27** does not increase the rate of electron transfer. Instead, the rate of electron transfer in **27** is decreased. It is clear that the electronic effect of the ethyl substituent is not additive by comparing the transition temperatures of **1**, **2**, **21**, **22**, and **27**: 365, 275, 195, 125, and >300 K, respectively. Further evidence can be gleaned from the electrochemical data of 1′,1‴-diethylbiferrocene, **19**, **20**, and **26**. These materials show two one-electron oxidation waves (Table IX). In a general way, electron-donating groups stabilize the ferrocenium cation, lowering the half-wave potential, and electron-withdrawing groups have the opposite effect. As a substituent, the ethyl group clearly acts as a net electron donor. It has been shown that the peak-to-peak separation ($\Delta E_{1/2}$) can gauge the interaction between

Table IX. Cyclic Voltammetry for Various Biferrocenes

compound	$E_{1/2}^a$ (V)	$E_{1/2}^b$ (V)	Δ^c (mV)	I_c/I_a^d
ferrocene	0.37		70	1.02
1′,1‴-diethylbiferrocene	0.20	0.36	68	1.01
	0.56		70	1.02
19	0.16	0.37	70	1.13
	0.53		71	1.01
20	0.15	0.37	67	0.97
	0.52		65	1.02
26	0.15	0.38	74	1.00
	0.53		63	1.07

[a] All half-wave potentials are reffered to the Ag^+/Ag electrode. [b] Peak separation between waves. [c] Peak-to-peak separation between the resolved reduction and oxidation wave maxima. [d] Peak–current ratio between cathode and anode.

two Fe sites.[35] The separations between the two oxidation waves for these materials are 0.36, 0.37, 0.37, and 0.38 V, respectively. In other words, the magnitudes of the electronic interactions between the two Fe atoms in **2**, **19**, **20**, and **26** are nearly equivalent in solution. Of course, this is not consistent with our solid-state variable-temperature ^{57}Fe Mössbauer results. We suggest that the difference in the rates of electron transfer of **2**, **21**, **22**, and **27** is a result of difference in the degree of tilting of the Cp rings from a parallel geometry.[36] The electronic ground state of ferrocene is a singlet, $^1A_{1g}$ ($e_{2g}^4a_{1g}^2$), where the one-electron molecular orbitals are predominantly d orbital in character: a_{1g} (d_{z^2}) and e_{2g} ($d_{x^2-y^2}$, d_{xy}).[37] As indicated by magnetic susceptibility[38] and EPR measurement,[39-41] the electronic ground state of ferrocenium is a doublet, $^2E_{2g}$ ($a_{1g}^2e_{2g}^3$). Lauher and Hoffmann have derived[27] the fragment orbitals for a bent $(Cp)_2M$ unit from the parallel geometry. Bending back the Cp rings splits the e_{2g} set into orbitals of a_1 ($d_{x^2-y^2}$) and b_2 (d_{xy}) symmetry. The a_{1g} orbitals rise rapidly in energy as the Cp rings are bent back. In this case, some metal $d_{x^2-y^2}$ character from a_1 mixes into a_1 (d_{z^2}) so that the torus of z^2 becomes hybridized away from the Cp rings. Hence, there is an increased ($d_{x^2-y^2}$, d_{xy})–ring overlap as the rings tilt. From Table VII, there is a correlation between the tilt angle and the rate of electron transfer in the series of biferrocenium triiodide salts. We suggest that the Cp rings in the cations of **1–13** are tilted by the hydrogen bond networks between the substituents and I_3^- anions, and e_{2g} metal orbitals are now bonding more with the tilted rings.

The impact of ring tilt could also explain why the physical properties of mixed-valence biferrocenium cations depend on the history of the sample. In the case of microcrystalline samples, various conformational arrangements in the alkyl substituents may induce different tilt angles.

Electron Paramagnetic Resonance. X-band EPR spectra were run at 77 K for samples of **21**, **22**, and **27**. An axial-type spectrum was observed for the series of compounds. Samples which were prepared by the two different preparations for a given cation gave essentially identical spectra. The g values evaluated from all of these spectra are collected in Table X, together with some g values from the literature.

For a mononuclear ferrocenium cation with no low-symmetry crystal field distortion, an axial-type spectrum will be observed with $g_\parallel = 6$ and $g_\perp = 0$.[39-41] As the low-symmetry crystal field increases, both $g_\parallel$ and $g_\perp$ approach a value of 2. In the case of a binuclear mixed-valence biferrocenium cation, the value of g

(35) Morrison, W. H., Jr.; Krogsrud, S.; Hendrickson, D. N. *Inorg. Chem.* **1973**, *12*, 1998.
(36) Lee, S. L.; Li, F. Y.; Dong, T.-Y. *Chem. Phys. Lett.* **1990**, *175*, 170.
(37) Duggan, D. M.; Hendrickson, D. N. *Inorg. Chem.* **1975**, *14*, 955.
(38) Hendrickson, D. N.; Sohn, Y. S.; Gray, H. B. *Inorg. Chem.* **1971**, *10*, 1559.
(39) Horsfield, A.; Wassermann, A. *J. Chem. Soc. A* **1970**, 3202.
(40) Prins, R.; Kortbeek, A. *J. Organomet. Chem.* **1971**, *33*, C33.
(41) Horsfield, A.; Wassermann, A. *J. Chem. Soc., Dalton Trans.* **1972**, 187.

Table X. Electron Paramagnetic Resonance Data[a]

compound	T (K)	$g_{\|\|}$	$g_\perp$	Δg[b]
2[c]	77	3.10	2.00	1.10
2[d]	77	3.11	2.00	1.11
21[c]	77	3.05	1.95	1.10
21[d]	77	3.09	2.00	1.09
22[c,d]	77	2.91	1.97	0.94
22[d]	77	3.10	2.00	1.10
27[c]	77	3.09	1.91	1.18
27[d]	77	3.10	1.92	1.18
1	4.2	3.58	1.72	1.86
4	4.2	2.98	1.92	1.06
5	4.2	3.02	2.01	1.07
			1.89	
6	77	3.23	1.94	1.29
7	77	3.14	1.91	1.23
9	77	2.97	1.95	1.02
10	77	3.10	1.93	1.17
11	4.2	2.75	2.01	0.76
			1.97	

[a] Powder sample. [b] $\Delta g = g_{\|\|} - g_\perp$. [c] Prepared by method 1. [d] Prepared by method 2. [e] Ground sample.

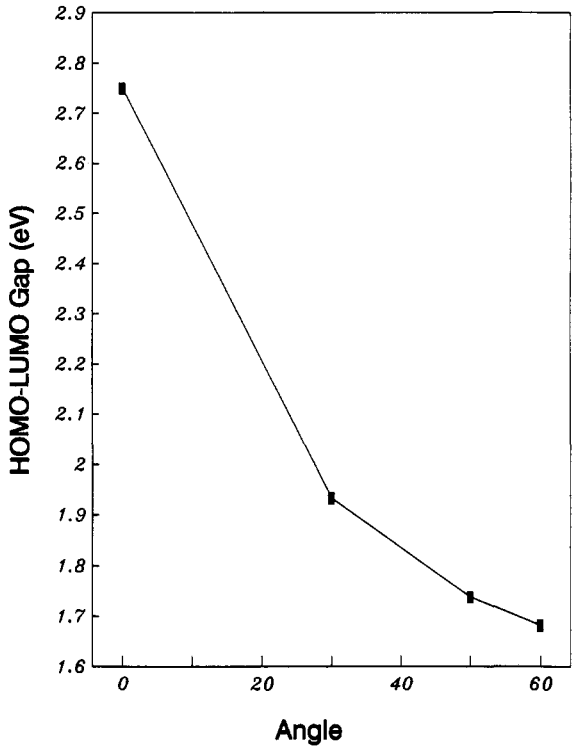

Figure 15. HOMO–LUMO gap as a function of tilt angle.

tensor anisotropy ($\Delta g = g_{\|} - g_\perp$) is considerably reduced. Hendrickson suggested[10] that this is a reflection of considerably reduced orbital angular momentum in the ground state that results from admixture of the $S = 0$ Fe(II) electronic configuration into the ground state. In general, if the Δg value for a given mixed-valence biferrocenium cation is smaller than 0.75,[10] then the rate of electron transfer is greater than the EPR time scale (10^9–10^{10} s^{-1}). From Table X, the Δg values of **21**, **22**, and **27** suggest that the cations in these compounds are localized on the EPR time scale at 77 K. Hence, it is consistent with the Mössbauer data. From Table X, it appears that there is no correlation between the values of Δg and temperatures for the delocalization–localization transition. We believe that this is mainly due to the contribution of low-symmetry crystal field distortion.

Effects of Ring Tilting. The goal of this section is to present an explanation for the differences of electron-transfer rates in the series of mixed-valence cations.

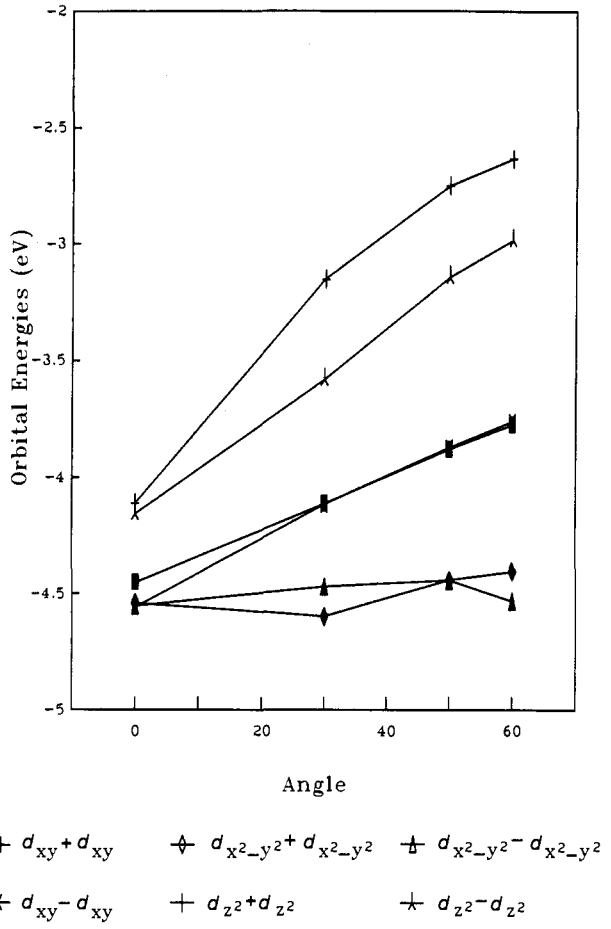

Figure 16. Fragment orbitals for bending biferrocenium triiodide from parallel geometry.

In Hendrickson's theoretical model,[42] the factors that are potentially important in controlling the rate of intramolecular electron transfer in a mixed-valence cation include (1) the effective barrier for electron transfer in the cation, (2) the effective barrier for charge oscillation in the anion, and (3) the intermolecular cation–cation and cation–anion interactions. A change in valence for a transition-metal complex is generally accompanied by a sizable coordination sphere reorganization. For an iron metallocene, the distance between Fe and the Cp ring centroid changes from 1.65 Å for Fe(II) to 1.70 Å for Fe(III). When an intramolecular electron transfer occurs in a biferrocenium cation, the two Cp rings bound to the Fe(II) ion move away from the metal to adjust their distance to the larger dimension appropriate for a $(Cp)_2Fe^{III}$ moiety. At the same time, the dimensions of the $(Cp)_2Fe^{III}$ moiety contract to those of a $(Cp)_2Fe^{II}$ species. In Hendrickson's model, the 3d electrons of the Fe ions couple strongly with this out-of-phase combination of Cp–Fe–Cp breathing modes. However, this conventional picture does not lead to net tilting of the Cp rings, and thus does not correlate with the tilt angles observed in the crystallography studies. In order to agree with our results based largely on X-ray data, the ring tilting must be considered in the Hendrickson micromodulation picture.

Albright has utilized a Walsh diagram to qualitatively describe the relationship between ring tilt and frontier orbital energy in $M(Cp)_2$ fragments.[43] The key feature of this diagram is the destabilization of the a_{1g} and e_{2g} orbitals accompanied by the lowering in energy of the e_{1g} orbitals as the tilt angle increases. For detailed information concerning the reactivities and general features of $M(Cp)_2$ fragments, one should refer to the original

(42) Kambara, T.; Hendrickson, D. N.; Dong, T.-Y.; Cohn, M. J. *J. Chem. Phys.* **1987**, *86*, 2326.
(43) Albright, T. A. *Tetrahedron* **1982**, *38*, 1339.

work of Lauher and Hoffmann.[27] In order to examine the effect of electron delocalization in the series of mixed-valence biferrocenium cations, we performed extended Hückel calculations[27] for tilt angles varying from 0 to 60° to see how the HOMO–LUMO gap ($E(e_{1g})$–$E(a_{1g})$) correlated with the tilt angle. As can be seen from Figure 15, the HOMO–LUMO gap decreases as the tilt angle increases. Figure 16 illustrates the fragment orbitals for bending of biferrocenium triiodide **1** from a parallel geometry. As can be seen in Figure 16, the $d_{z^2} \pm d_{z^2}$ and $d_{xy} \pm d_{xy}$ orbitals rise rapidly in energy as the Cp rings are bent back. In other words, the metal nonbonding orbitals start to interact with the ligand π orbitals. Hence, bending back the Cp rings leads to a larger extent of metal–ligand interactions which render intramolecular electron transfer much more facile.

Concluding Comments. In this paper, we demonstrate that relatively minor perturbations caused by the substituents on the Cp ring have pronounced effects on the electronic structure and rate of intramolecular electron transfer. The observed tilt angles and the critical temperatures for the electron localization–delocalization transition are clearly correlated. Our data indicates that Cp ring tilting plays a crucial role in intramolecular electron transfer in biferrocenium cation systems. The substituents in the series of biferrocenium cations modify the local structure of the ferrocenyl moiety and lead to stronger metal–ligand interaction. The adding of ring tilting to the original micromodulating mechanism needs to be considered.

Acknowledgment. Acknowledgments are made to the National Science Council, Taiwan, ROC, and Institute of Chemistry at Academia Sinica for financial support.

Supplementary Material Available: Complete tables of positional parameters, bond lengths and angles, and thermal parameters for **19**, **20**, and **22** (12 pages); tables of observed and calculated structure factors for the same three compounds (24 pages). Ordering information is given on any current masthead page.